NUCLEAR SCIENCE AND ENGINEERING

DOI: https://doi.org/10.1080/00295639.2021.1961542

Measurements of Neutron Scattering from a Copper Sample Using a Quasi-Differential Method in the Region from 2 keV to 20 MeV

E. Blain,[a]* Y. Danon,[a] D. P. Barry,[b] B. E. Epping,[b] A. Youmans,[a] M. J. Rapp,[b] A. M. Daskalakis,[b] and R. C. Block[a]

[a]*Rensselaer Polytechnic Institute, Gaerttner LINAC Center, Troy, New York 12180*
[b]*Naval Nuclear Laboratory, P.O. Box 1072, Schenectady, New York 12301-1072*

Received May 6, 2021
Accepted for Publication July 26, 2021

Abstract — *Neutron scattering from a copper sample was measured at Rensselaer Polytechnic Institute utilizing the quasi-differential method. The measurement spanned the energy range from 0.5 to 20 MeV using the high-energy scattering system and from 2 keV to 0.5 MeV using the new mid-energy scattering system. Copper was selected as a material of interest to measure due to large discrepancies between experiments and simulations of the Zeus benchmark. The Zeus benchmark consists of a copper reflected highly enriched uranium system, and the angular distribution of copper scattering was thought to potentially be the cause of the discrepancy. The copper measurements found differences in the scattering response particularly in the incident energy region from 1 to 2 MeV for the high-energy measurement and from 2 to 4 keV in the mid-energy system. These differences are particularly noticeable at angles near 90 deg in the high-energy system and back angles in the mid-energy system. Additionally, for ENDF/B-VIII.0 there is a large discrepancy at the forward angle in the energy range around 0.5 MeV. For these reasons, a new evaluation of copper scattering utilizing these results is recommended and perhaps could help to improve the agreement with the Zeus benchmarks.*

Keywords — *Neutron scattering, copper, Zeus benchmark, angular distribution, nuclear data..*

Note — *Some figures may be in color only in the electronic version.*

I. INTRODUCTION

Accurate simulation and modeling of nuclear systems comprise an integral part of many aspects of nuclear power and engineering including reactor simulations, criticality safety, nuclear safeguards, and nonproliferation. These simulations rely on a combination of theoretical models and nuclear data in order to accurately simulate nuclear systems. Therefore, having nuclear data with low uncertainty is essential to the accuracy of the simulation codes.

Nuclear data are contained in evaluated nuclear data files that are generated by different evaluations around the world. Some of the most prominent evaluations are the Evaluated Nuclear Data File[1] (ENDF), maintained by the Cross Section Evaluation Working Group; the Joint European Fusion Fission (JEFF) library,[2] maintained by the European Nuclear Energy Agency; and the Japanese Evaluated Nuclear Data Library[3] (JENDL), maintained by the Japanese Nuclear Data Committee. While these libraries are often in agreement on their evaluations, there are many times where the different evaluation projects produce differing nuclear data for a given isotope or reaction.

In an attempt to assist in determining which library is most accurate and provide data for future evaluations, the quasi-differential scattering method was developed at Rensselaer Polytechnic Institute[4] (RPI). This method relies on performing a neutron scattering measurement

*E-mail: blaine2@rpi.edu

and comparing it with detailed simulations of the experiment in order to determine which nuclear data library used in the simulations most accurately represents the experimental data. Additionally, the comparison can provide information in regions where none of the evaluations accurately model the data to identify areas that could be improved in future evaluations.

This method has previously been used for Fe, Be, Mo, Zr, and Pb (Refs. 5 through 8), and recently, an experiment using ^{238}U (Ref. 9) was used by the International Atomic Energy Agency to assist with its new evaluation of ^{238}U scattering.[10] This methodology has been extended to lower-energy neutrons using A Multi Angle Neutron Detection Array (AMANDA) to extend the low energy of the measurement range from 0.5 MeV to 2 keV. An experiment was performed using these systems to investigate the neutron scattering from a natural sample of copper.

Copper was selected as a material of interest primarily because of its importance in specific critical benchmarks. Critical benchmarks are experimental systems that precisely measure the criticality of a system. Detailed simulations of these benchmarks are compared to the experimentally measured values and are used as part of the validation of simulation codes and nuclear data libraries. However, when an update is made to either the nuclear data or the simulation physics, sometimes certain benchmarks do not perform accurately.

In the most recent ENDF/B-VIII.0 evaluation, the simulations of the Zeus benchmarks performed poorly.[11] The Zeus benchmarks consist of a copper reflected highly enriched uranium (HEU) system.[12] In the Zeus 1 benchmark, the copper plates are interspersed with graphite, and in the Zeus 6 benchmark, the copper plates are interspersed with steel plates. The Zeus 5 benchmark has stacked HEU plates and a copper reflector. The Zeus 5 and Zeus 6 benchmarks are fast spectrum benchmarks, and the Zeus 1 benchmark is an intermediate spectrum benchmark. The differences in the benchmark and the simulation were thought to have occurred due to uncertainties in the scattering cross sections and particularly in the angular distribution of copper scattering.[11]

A sensitivity study was performed on the Zeus benchmarks using the DICE code[13] and showed which cross sections are most sensitive in which energy regions, shown in Fig. 1 for ^{63}Cu and Fig. 2 for ^{65}Cu. The sensitivity represents the change in k_{eff}, the criticality of the system, for the benchmark relative to a change in the respective cross section of the material in the simulation. Larger sensitivities correspond to materials of significance within the benchmark. This clearly shows that the most sensitive copper cross section for this benchmark is the scattering cross section and that there is high sensitivity particularly in the region around 1 MeV. Therefore, a new, more accurate, measurement of scattering from copper will help in constraining the copper scattering response, and if large deviations are found between the simulation and the experiment,

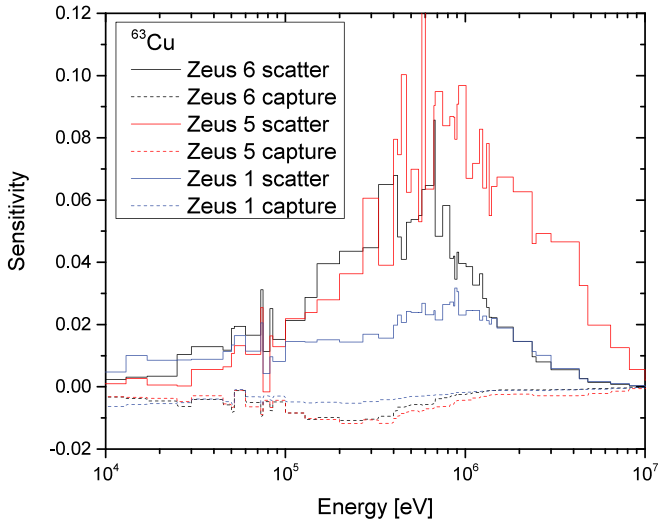

Fig. 1. The sensitivity of the Zeus 1, Zeus 5, and Zeus 6 benchmarks to the scattering and capture cross sections for ^{63}Cu. This highlights a very high sensitivity to the scattering cross section indicating that changes to the scattering cross section will cause greater impact than changing the capture cross section.

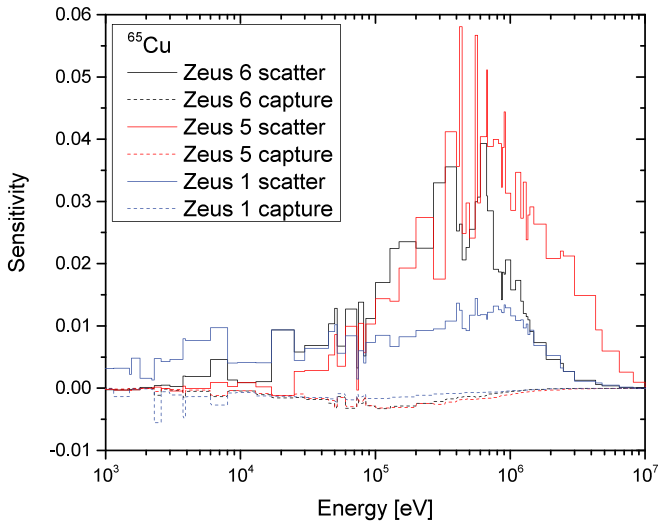

Fig. 2. The sensitivity of the Zeus 1, Zeus 5, and Zeus 6 benchmarks to the scattering and capture cross sections for ^{65}Cu. This highlights a very high sensitivity to the scattering cross section indicating that changes to the scattering cross section will cause greater impact than changing the capture cross section.

information can be obtained about how the nuclear data may be improved to reduce the difference in the benchmark.

II. METHOD

The quasi-differential scattering method compares an experimental measurement with detailed simulations, utilizing different nuclear data libraries, in order to accurately determine which evaluation best matches the experiment. A carbon sample, the cross sections and angular distributions of which are well known, is measured in addition to the sample of interest. The carbon sample is used to validate the method as well as to calculate the normalization value between the experiment and simulation. Additionally, the comparison between the measured sample and simulations gives insight into which energy regions of the cross section and angular distributions can be improved in future nuclear data evaluations.

In order to accurately simulate the experiment, there are three key components that need to be well known: the experimental geometry, the incident neutron flux from the accelerator beam, and the detector response or efficiency. These have been determined for both experimental systems and are detailed below.

II.A. Geometry

Accurate representation of the experimental geometry is essential for a comparison between the experimental measurement and the simulation. One of the most important features for the simulation is the neutron beam travel from the neutron-producing target to the scattering sample. This includes the beam collimation and transmission through any beam filters that were used in the experiment. Both the high-energy (mega-electron-volt) measurements and mid-energy (kilo-electron-volt) measurements had a well-collimated beam resulting in a 3-cm beam radius at the sample. For the mid-energy measurement, the beam filters included a 0.794-cm-thick (5/16-in.-thick) B_4C overlap filter in order to remove thermal region neutrons from the previous accelerator pulse and 0.635 cm (0.25 in.) of lead in order to reduce the gamma flux incident on the sample. For the high-energy run, there was no need for an overlap filter, and for the gamma filter, 1.905 cm (0.75 in.) of ^{238}U was used. In addition to the beam filters and collimation, accurate modeling of the sample as well as scattering materials around the sample is necessary. These include the walls, floor, central beam pipe, and experimental table, all of which contribute to the scattered signal at the detector location.

II.B. Incident Flux

Accurate simulations of the experimental system rely heavily on knowing the flux incident on the scattering sample. In order to determine the incident flux, a measurement was made at the scattering sample position using a ^{235}U fission chamber. Since the fission cross section of ^{235}U is well known, the flux shape can be determined from the measurement using Eq. (1):

$$\phi(E_i) = \frac{C_i - B_0}{N \cdot \sigma_{235}(E_i) \cdot trigs \cdot \eta_i \cdot \Delta E_i} \quad , \tag{1}$$

where

C_i = counts from the fission chamber in time-of-flight bin i

B_0 = constant room background

N = number density of ^{235}U

$\sigma_{235}(E_i)$ = ^{235}U cross section

$trigs$ = number of accelerator start triggers

η_i = detector efficiency

ΔE_i = width in energy of the corresponding time-of-flight bin i.

While the detector efficiency of the chamber is unknown and it is therefore impossible to get the absolute flux, the simulations only require the flux shape, which can then allow the simulations to be normalized to the experimental results.

Two separate measurements were performed in order to obtain the incident flux for the high-energy and mid-energy systems and can be found in the Ref. 14 for the high-energy system and in Fig. 3 for the mid-energy system. The count rate in the detector is corrected for dead time and background and by the transmission of the neutron beam through the various beam filters in the measurement in order to obtain the flux at the neutron source location. This allows for different beam filters to be used between the flux measurements and the experiment as long as the experimental beam filters are accurately modeled.

II.C. Efficiency

In addition to accurate geometry and flux for the simulation, the detector response needs to be accurately simulated. This is achieved through Monte Carlo N-Particle[16] (MCNP) simulations utilizing a tally

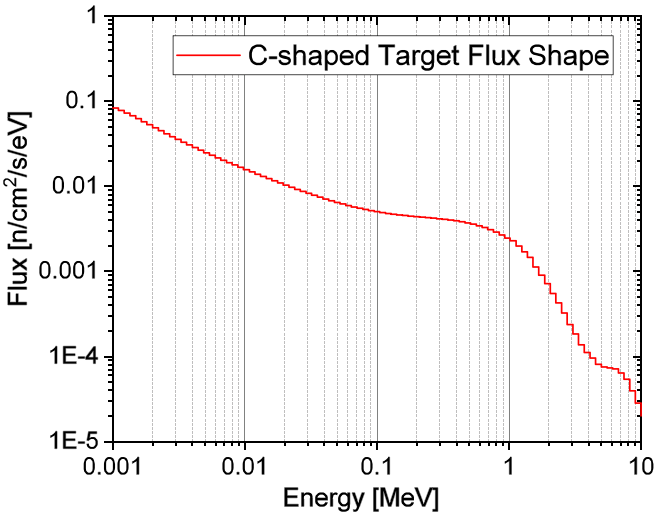

Fig. 3. The flux used for the mid-energy scattering simulation for the Li-glass detector array from the C-shaped neutron target[15] at the RPI LINAC.

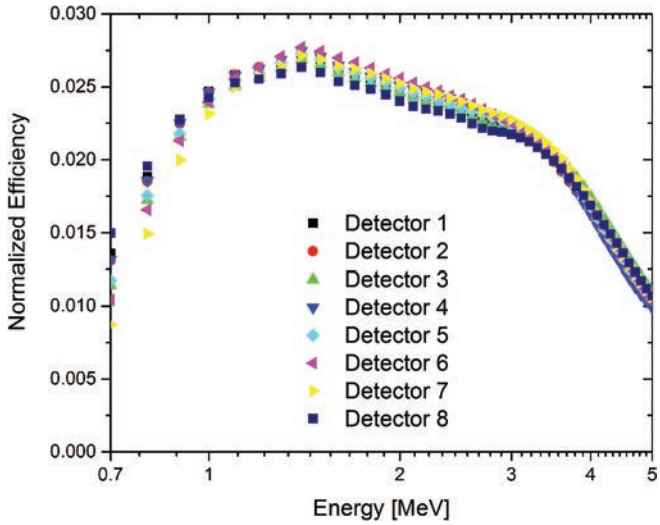

Fig. 4. The relative efficiencies for the eight high-energy detectors. These efficiencies are used in the simulation of the high-energy scattering system.

multiplier card that multiplies the tally by the probability of detection at a given incident neutron energy. Therefore, the response of the detector to neutrons, referred to as the neutron efficiency, needs to be known for each detector in the simulation. This efficiency was directly measured for the high-energy array and simulated for the mid-energy array. The specifics of the efficiency determination for each system are as follows.

The high-energy array utilizes EJ-301 liquid scintillators for neutron detection in the energy range from 20 to 0.5 MeV. Each detector's relative efficiency was determined by placing it directly in the neutron beam and measuring counts as a function of time of flight. The time-of-flight technique was used to convert the neutron flight time to corresponding incident neutron energy. Knowing the flux shape from the previous measurements with the ^{235}U chamber, the detection efficiency shape was found for each individual detector as a function of incident neutron energy. Additionally, the same pulse shape discrimination techniques for the data processing, discussed in Sec. IV, are used when determining the detector efficiency. This is primarily important since the efficiency drops dramatically above 3 MeV where detector pulses saturate the digitizer and gamma neutron discrimination can no longer be performed for neutrons that deposit greater than 3 MeV in the detector. The individual detector efficiency shapes for all eight detectors can be seen in Fig. 4.

For the mid-energy array, ^{6}Li-glass scintillators were used for neutron detection, and the same method for determining efficiency was attempted. However, because of the large gamma sensitivity and low overall efficiency of the Li glass, the in-beam measurement method was not practical for these detectors. Instead, the detector response was simulated using the MCNP simulation code with different monoenergetic neutron sources incident on a cell of Li glass. The detection efficiency as a function of incident neutron energy was then found and can be seen in Fig. 5. It is important to accurately model the efficiency even at energies below the 1-keV low-energy threshold of the system since scattered neutrons

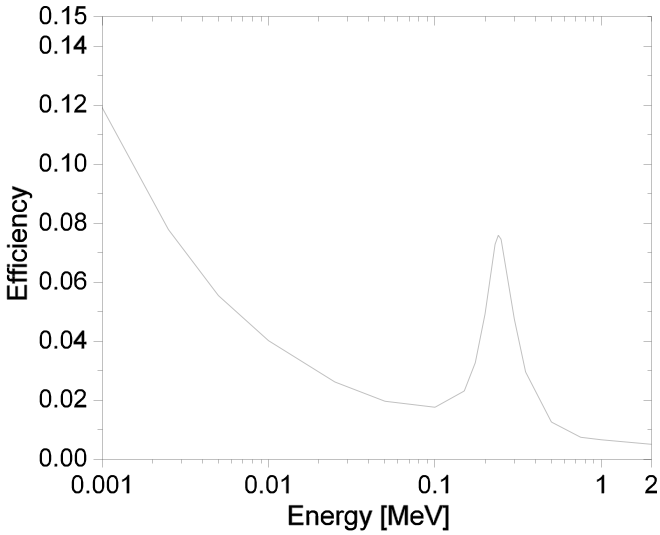

Fig. 5. The simulated detector efficiency for the ^{6}Li-glass detectors. This shows the large peak around 300 keV corresponding to a broad resonance in the ^{6}Li cross section.

will have a lower incident energy and the room background will not be accurately simulated without including these energies.

III. EXPERIMENTAL DETAILS

The copper scattering experiments were performed at the RPI Gaerttner Linear Accelerator (LINAC) Center. The LINAC is a 60-MeV electron linear accelerator that creates neutrons through a photoneutron reaction in a Ta target. This creates a white, isotropic source of neutrons that is then collimated down evacuated flight paths to measurement stations located at different flight path distances from 15 to 250 m. Different neutron production targets can be used with different moderator configurations in order to shift the flux to different energy regions. These experiments used both an unmoderated bare target[15] for the high-energy region and a C-shaped target[15] that used additional water moderation to increase the neutron flux in the kilo-electron-volt energy region. Specific experimental configurations for the two measurements are as follows.

III.A. High-Energy Experiment

The high-energy measurement utilized the RPI high-energy scattering system,[4] which consists of an array of eight EJ-301 liquid scintillators located at various angles around a scattering sample as seen in Fig. 6. The center of the array is located 30.07 m from the neutron source, and the detectors are at a distance of 0.5 m from the scattering sample. The uncertainty in the total flight path was 0.005 m. Two weeks of measurements were performed, and the angles of the detectors for each week can be found in Table I. The angular uncertainty for each angle was 3 deg. The dimensions and masses of the scattering samples are given in Table II.

A measurement cycle consisted of open beam, graphite standard, and copper sample measurements with each sample being measured for 15 min/cycle. The signals from the detectors were connected to an 8-bit Acquiris AP240 digital data acquisition board that operated at a 1-GHz sampling rate resulting in 1-ns timing resolution. The neutron beam was collimated to a beam radius of 3 cm, and a 1.905-cm-thick ^{238}U filter was used to reduce gamma flux on the scattering sample.

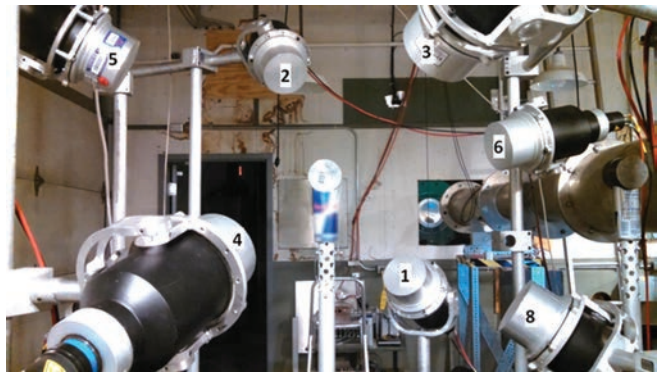

Fig. 6. The high-energy scattering array showing the labeled eight EJ-30l detectors surrounding the scattering sample on the low mass sample holder in the center of the array.

TABLE I

Detector Angles

Detector Number	Week 1 Angle	Week 2 Angle
1	90 ± 3	107 ± 3
2	52 ± 3	73 ± 3
3	26 ± 3	31 ± 3
4	52 ± 3	73 ± 3
5	90 ± 3	107 ± 3
6	119 ± 3	141 ± 3
7	154 ± 3	155 ± 3
8	119 ± 3	141 ± 3

III.B. Mid-Energy Experiment

The mid-energy experimental setup utilized the AMANDA array, which consists of eight ^{6}Li-glass and

TABLE II

Sample Measurements

Sample	Diameter	Thickness	Mass
Copper	7.628 ± 0.001 cm	2.99 ± 0.03 cm	1225.1 ± 0.1 g
Carbon	7.499 ± 0.001 cm	7.005 ± 0.001 cm	521.87 ± 0.01 g

two ^{7}Li-glass scintillators seen in Fig. 7. The center of the array is located 32.24 m from the neutron scattering source, and the detectors are located 0.25 m from the scattering sample. The detector angles are listed in Table III, and the two ^{7}Li detectors were moved halfway through the run to allow for ^{7}Li measurements to be performed at all scattering angles. For all other detectors there were two detectors at each scattering angle but at different ϕ angles.

The samples used were the same as those in the high-energy measurement, and their dimensions are in Table II. The detector signals were input into a Struck SIS3316 digitizer board that operated at a sampling rate of 250 MHz. The beam was collimated to a radius of 3 cm, and a 0.5-in.-thick lead filter was used to reduce the gamma flux on the detector along with a 0.79375-cm-thick B_4C filter that was used as an overlap filter so that neutrons from the previous LINAC pulse did not contaminate the signal.

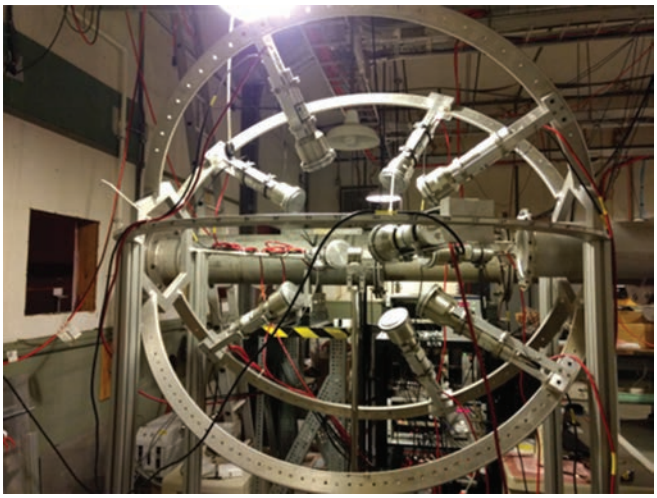

Fig. 7. The mid-energy scattering array with eight ^{6}Li and two ^{7}Li detectors surrounding a scattering sample. The radius of the array is 0.25 m.

TABLE III

Detector Angles

Detector	Theta Angle	Phi Angle	Detector Type
1	35	300	^{6}Li
2	35	60	^{6}Li
3	70	0	^{6}Li
4	70	120	^{6}Li
5	115	300	^{6}Li
6	115	60	^{6}Li
7	150	0	^{6}Li
8	150	180	^{6}Li
9	35/70	180	^{7}Li
10	150/115	240	^{7}Li

IV. DATA ANALYSIS

For both experiments, data were taken with a digital data acquisition system and then processed into a finalized form that can then be compared to the detailed MCNP simulation. The processing steps for each method are as follows.

IV.A. High-Energy Experiment

The experimental data for each of the eight high-energy EJ-301 detectors were sent through an Acqiris AP-240 digitizer board, and the digital data were stored in a binary format for processing. The processing of the data involved improvement of pulse timing through constant fraction discrimination techniques and correction for t_0 of the neutron pulse, and each pulse was classified as either a neutron or a gamma event based on a pulse shape classification technique.[5] Time t_0 is defined as the birth time of the neutrons and is determined by measuring the timing of the gamma burst created at the target during neutron production. The t_0 value for the measurement was found to be 1824 $\pm$ 3 ns. Accurate pulse shape discrimination is essential for comparing to detailed simulations since the simulation assumes that the given flux at a location is solely from neutron events.

In order to achieve better pulse shape discrimination, a gamma misclassification correction previously developed at RPI (Ref. 5) was employed to remove gamma signals falsely classified as neutrons. Following this classification, the neutron counts as a function of time of flight for each detector are obtained and can then be compared to the simulation.

When comparing the simulation to the experimental data, it is important that the comparison be as direct as possible. Therefore, the simulation and the experiment are both subtracted by their corresponding open (background) run. For the simulation this is achieved by running a simulation without the sample and doing a direct subtraction. For the experimental data, a no sample or open run is cycled with the copper and graphite runs, which can then be subtracted. It is important to correct for any differences in the neutron beam output between the open runs and the copper runs. This is achieved through the use of neutron beam monitors, which are ^{235}U fission

chambers that monitor the neutron beam intensity throughout the experiment. Once this correction is applied, the open subtracted neutron counts from the sample can be obtained using Eq. (2) with a corresponding statistical uncertainty given by Eq. (3) (Ref. 5):

$$C_{i,j} = (D^S_{i,j} - G^S_{i,j}) - (D^O_{i,j} - G^O_{i,j}) \cdot \frac{M^S}{M^O} \tag{2}$$

and

$$\Delta C_{i,j} = (D^S_{i,j} + (\Delta G^S_{i,j})^2 + D^O_{i,j}\left(\frac{M^S}{M^O}\right)^2 + (\Delta G^O_{i,j})^2\left(\frac{M^S}{M^O}\right)^2 + M^S\left(\frac{D^O_{i,j} - G^O_{i,j}}{M^O}\right)^2 + (D^O_{i,j} - G^O_{i,j})^2\frac{(M^S)^2}{(M^O)^3})^{0.5}\ , \tag{3}$$

where

$D^S_{i,j}$ = counts in the sample

$G^S_{i,j}$ = gamma misclassification correction for the sample counts

$D^O_{i,j}$ = counts in the open

$G^O_{i,j}$ = gamma misclassification correction for the open counts

M^S = monitor counts for the sample

M^O = monitor counts for the open

$\Delta G^O_{i,j}$, $\Delta G^S_{i,j}$ = uncertainties in the gamma misclassification, which can be found in Ref. 14.

The final step necessary for a comparison between the simulation and the experiment is to determine the normalization value between the simulation and the experiment.

Following the processing of the raw data files, processed files were generated for the open, carbon, and copper measurements, and the data for each sample were summed over the course of the run. When performing a comparison between the simulation and the experiment, the magnitudes of the two distributions are very different, and a normalization factor needs to be determined for an accurate comparison to be made. In order to find this value, the Open subtracted carbon sample was compared to an Open subtracted carbon simulation. For this purpose, carbon scattering is treated as a standard in this region, and therefore, a normalization value can be obtained by finding the value that minimizes the total uncertainty between the carbon simulation and experiment.

During this analysis it was identified that detectors 3 and 4 had issues for normalization values. During the experiment there were issues with the data acquisition board for detectors 3 and 4, and this may have resulted in inaccurate experimental data being recorded. For these reasons detectors 3 and 4 were not included in the analysis or in the quantification of the uncertainty normalization.

Figure 8 shows the individual detector normalization values for both weeks for all detectors used in the analysis. This shows that for the copper measurement, a normalization value was found that resulted in an average uncertainty of 4.1% for the first week and 3.3% for the second week for the carbon sample. The normalization value can then be used to normalize the copper measurement and compare it to the copper simulation. The uncertainty for the normalization was used as the systematic uncertainty and was added linearly to the statistical uncertainty to obtain the overall uncertainty values for the experiment.

IV.B. Mid-Energy Experiment

Similar to the high-energy system, the data from each of the Li-glass detectors were recorded with a digitizer

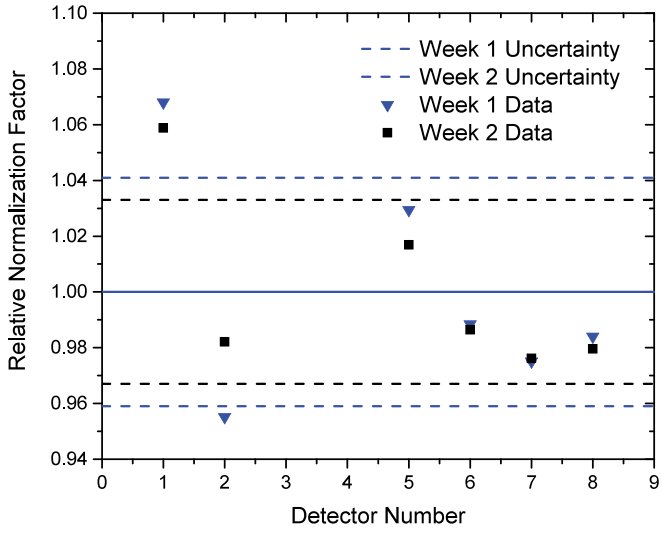

Fig. 8. The relative normalization values for both weeks of the high-energy measurement. Detectors 3 and 4 were removed due to issues with the experimental data. The dashed lines show the standard deviation of the datasets for each week.

board, and the pulse waveforms were saved in a binary data format. The integral of the pulse was calculated for each pulse, and the timing of the pulse was found using the constant fraction discrimination method. A pulse integral method was used to determine valid neutron events, and an example of the pulse integral values for a measurement can be seen in Fig. 9. Pulses with integrals between 10 000 and 18 000 were classified as neutron events, and all other events were removed. The data were then corrected for the time zero of the events based on the gamma flash timing in order to obtain neutron counts as a function of time of flight. This resulted in a time-of-flight histogram of the neutrons, which could then be compared to the MCNP simulations of the experiment.

While the pulse integral discrimination works well for identifying the valid neutron events, there are also gamma events that are present in this integral region. In order to accurately subtract out the gamma signal, a ^{7}Li detector was placed at each of the scattering angles during the experiment. Lithium-7 has the same gamma response as the ^{6}Li-enriched detectors; however, it has no neutron response due to the lack of ^{6}Li. This allows for measurements to be performed using both the ^{7}Li and ^{6}Li detectors where the gamma signal can be measured from the ^{7}Li detectors and subtracted from the ^{6}Li. This is displayed in Fig. 9, which shows a pulse integral response from one of the ^{6}Li and ^{7}Li detectors at the same angle. This demonstrates that above and below the neutron peak, the detectors have the same response indicating that they have the same gamma response, and this

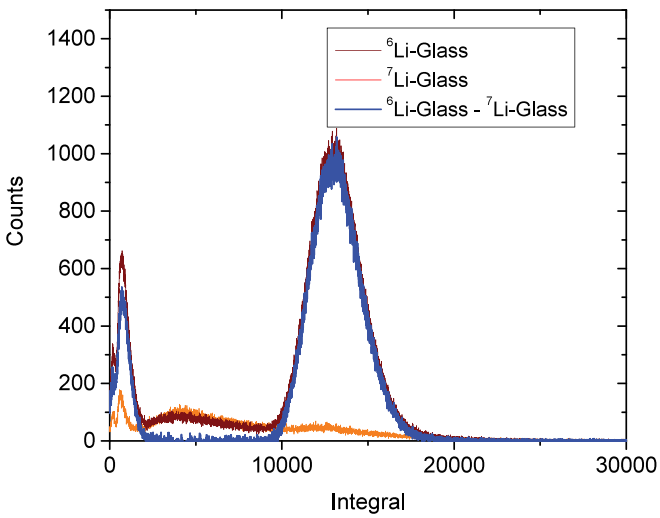

Fig. 9. Pulse integral plot for a ^{6}Li detector and a ^{7}Li detector at the same location with the net subtracted counts showing how ^{7}Li can be used to obtain the neutron only counts from the ^{6}Li detector.

can then be subtracted from the ^{6}Li to obtain the response only from neutron events.

The net neutron counts for each time-of-flight bin can be found using Eq. (4):

$$C_i = \left(D_i^{6S} - D_i^{7S} \times \frac{M^{6S}}{M^{7S}}\right) - \left(D_i^{6O} - D_i^{7O} \times \frac{M^{6S}}{M^{7S}}\right) \cdot \frac{M^{6S}}{M^{6O}} \quad , \tag{4}$$

where

D^{6S} = sample counts from the ^{6}Li detector

D^{7S} = sample counts from the ^{7}Li detector

D^{6O} = open counts from the ^{6}Li detector

D^{7O} = open counts from the ^{7}Li detector

M^{6S}, M^{7S}, M^{6O}, M^{7O} = monitor counts from the sample run for the ^{6}Li detector, monitor counts for ^{7}Li detector for the sample run, monitor counts for the ^{6}Li detector for the open run, and monitor counts for the ^{7}Li detector for the open run, respectively.

When comparing with the MCNP simulation, it is important to accurately subtract any gamma signal since the simulation records only the neutron flux at the detector location. The simulation therefore has a different equation for calculating the net neutrons in the simulation since the aspects of monitor normalization and gamma subtraction do not need to be taken into account, and therefore, it is the straight subtraction of the sample in simulation by the open simulation.

Similar to the high-energy measurement, the mid-energy copper simulation was normalized to the experiment using the carbon. The carbon simulation and experiment are open subtracted consistent with Eq. (4), and a normalization value is found that reduces the uncertainty between the simulation and the experiment. However, unlike with the high-energy normalization, each detector has its own normalization value. The detectors had a larger variation in counts that was attributed to different efficiencies due to differences in ^{6}Li content in the glass. Unlike

with the EJ-301 detectors, which could be measured directly in the neutron beam, the Li-glass detectors relied on simulation. While the simulation provides an accurate efficiency shape, the total efficiency is different for each detector. Therefore, each detector was individually normalized to its own carbon response, and that normalization value was used for the copper response.

Additionally, the normalization values were multiplied by the ratio of monitor counts from the copper sample to the carbon sample so that the normalization value can be adjusted for changes in beam conditions similar to the open monitor ratio. The spread of normalization values can be found in Fig. 10 highlighting the large normalization spread. The standard deviation of the normalization values was found and taken as the systematic uncertainty of 6.1% for the system. This uncertainty was linearly added to the statistical uncertainty to obtain the total experimental uncertainty.

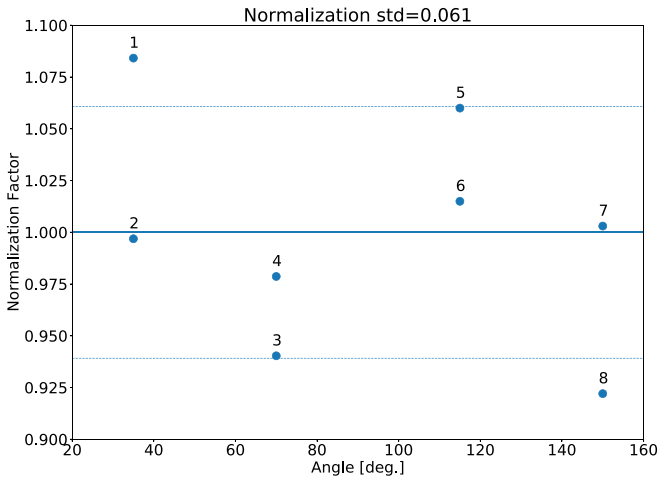

Fig. 10. The relative normalization values for the Li-glass detectors. This highlights the spread in the individual normalization values that result in a 6.1% systematic uncertainty.

V. RESULTS

V.A. High-Energy Experiment

Once the data have been fully processed, the experimentally measured detector response is compared to the simulated response using multiple nuclear data libraries for the sample of interest. For all other materials in the simulation, including the beam filters and surrounding environment, the ENDF/B-VIII.0 evaluation was used. Figure 11 shows a comparison of the carbon scattering data at an angle of 52 deg to the simulation. This shows good agreement between the

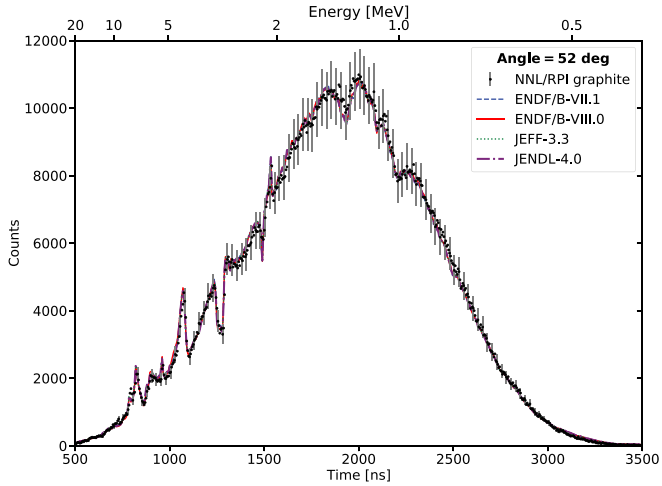

Fig. 11. The detector response for neutron scattering at an angle of 52 deg from the graphite reference compared with an MCNP simulation. There is good agreement between the simulation and experiment validating the method for this measurement.

simulation and experiment thus validating the method for this measurement. Figures 12, 13, and 14 show the comparison of the experimental data for the scattering from the copper sample and the MCNP simulations for angles at 52, 119, and 154 deg, respectively. These three angles were selected as a representative sample of all the data measured in the experiment.

For the copper sample there are two main regions of interest that show differences. The first is between 1

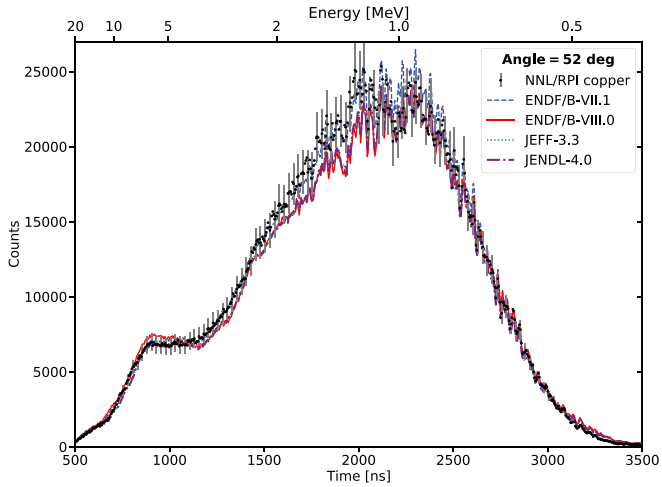

Fig. 12. The detector response for neutron scattering at an angle of 52 deg from the copper sample compared with MCNP simulations using various nuclear data libraries. There is general agreement between the simulations and experiment for the copper sample; however, there is a noticeable difference in the energy range from 1 to 2 MeV for all evaluations.

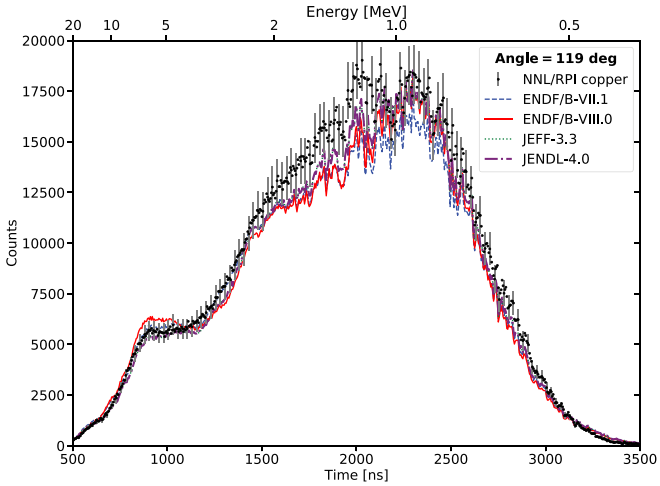

Fig. 13. The detector response for neutron scattering at an angle of 119 deg from the copper sample compared with MCNP simulations using various nuclear data libraries. There is general agreement between the simulations and experiment for the copper sample; however, there is a noticeable difference in the energy range from 0.8 to 3 MeV for all evaluations.

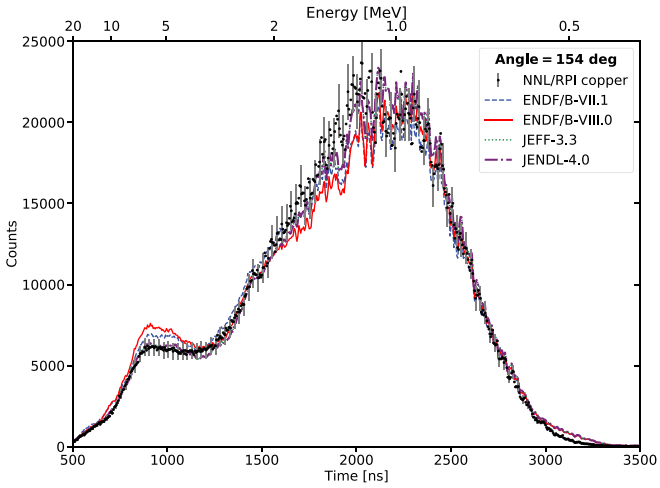

Fig. 14. The detector response for neutron scattering at an angle of 154 deg from the copper sample compared with MCNP simulations using various nuclear data libraries. There is general agreement between the simulations and experiment for the copper sample; however, there is a noticeable difference in the energy range from 1 to 2 MeV for all evaluations. Additionally, there is a difference between the simulations using the ENDF evaluation and the experimental data at 5 MeV.

and 2 MeV for all angles, and the second is the peak around 5 MeV. For all angles the data in the region between 1 and 2 MeV are greater than any of the evaluations, and this is most evident at the side angle of 119 deg shown in Fig. 13. The ENDF/B-VII.1 (Ref. 17) evaluation is actually the closest in this region; however, the JEFF 3.3, JENDL 4.0, and ENDF/B-VIII.0 evaluations are all much lower than the data. This indicates a region where a reevaluation of the evaluations could improve the agreement to the measured data. The second region of interest is the peak around 5 MeV, which is evident at 119 deg, Fig. 13, and 154 deg, Fig. 14. At these angles, again, the ENDF/B-VIII.0 evaluation has the worst comparison, and the JEFF 3.3 and JENDL 4.0 libraries fit this region much better.

V.B. Mid-Energy Experiment

Following the processing of the mid-energy data, the simulations were compared to the processed experimental data in order to identify any discrepancies between the experiment and simulation. Figure 15 shows the comparison of the carbon simulation with the experimental data showing good agreement between the two and highlighting the validity of the method. For the copper sample, the experimental data were compared to simulations using the ENDF/B-VIII.0, JEFF 3.3, and JENDL 4.0 libraries. All other materials in the simulations, such as the surrounding environment and beam filters, used the ENDF/B-VIII.0 library. Figures 16, 17, and 18 show the comparison of the experimental data with the simulations in the energy range from 0.5 MeV to 2.5 keV for detectors at angles 35, 115, and 150 deg, respectively.

The copper simulations overall show a good agreement between the experiment and simulations with two

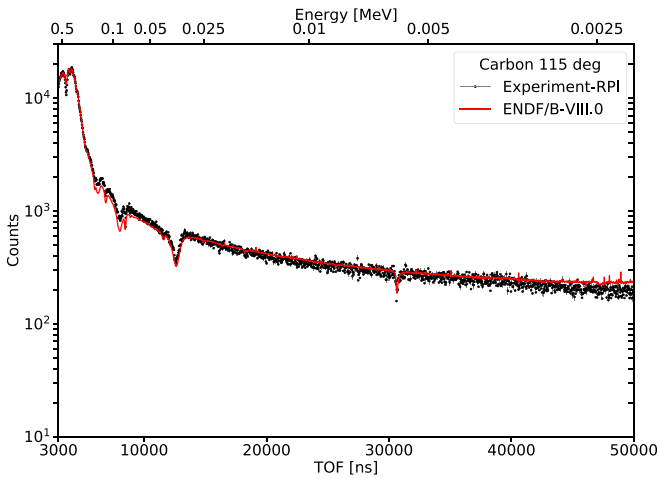

Fig. 15. The detector response for neutron scattering at an angle of 115 deg from a carbon sample compared with an MCNP simulation. There is good agreement between the simulation and experiment highlighting the validity of the method.

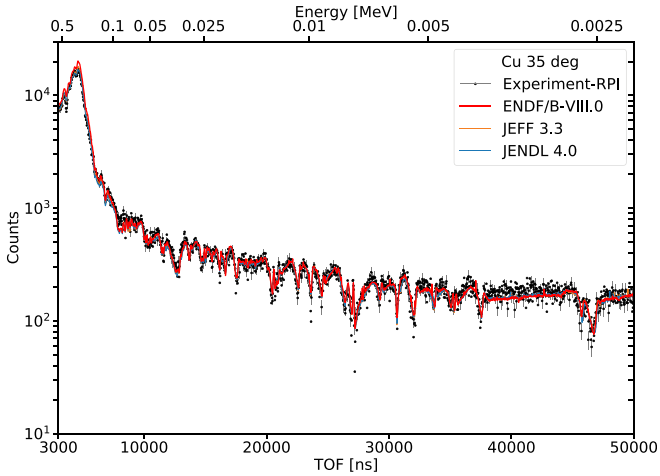

Fig. 16. The detector response for neutron scattering at an angle of 35 deg from a copper sample compared with MCNP simulations using various nuclear data libraries. There is general agreement between the simulation and experiment; however, there is a noticeable difference around 300 keV for the ENDF evaluation. This may indicate a region of potential improvement in the next ENDF evaluation for copper.

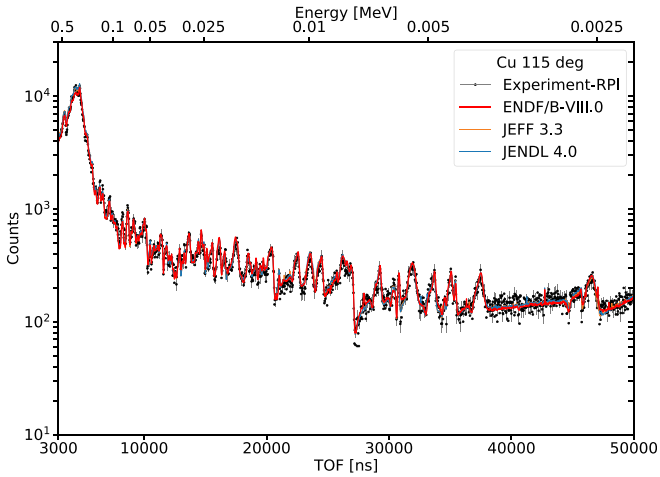

Fig. 17. The detector response for neutron scattering at an angle of 115 deg from a copper sample compared with MCNP simulations using various nuclear data libraries. For this angle there is good agreement between the copper sample and simulation. This comparison also shows that the experiment can accurately reproduce the resonance structure of the simulation and may be used for resonance measurement in the future.

noticeable points of discrepancy. At 35 deg there is a difference near 300 keV where the simulation using the ENDF evaluation is much higher than the experimental data. The JEFF 3.3 and JENDL 4.0 libraries follow the data much more closely in this region, and this may indicate a region of improvement in future ENDF evaluations of carbon. The

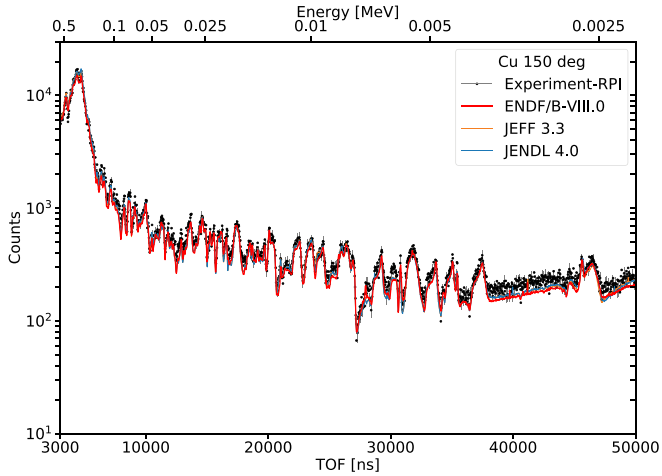

Fig. 18. The detector response for neutron scattering at an angle of 150 deg from a copper sample compared with MCNP simulations using various nuclear data libraries. There is general agreement between the simulation and experiment; however, there is a noticeable difference in the energy range from 2.5 to 4 keV for all evaluations. In this region the experimental data are higher than any of the evaluations.

115-deg detector shows good agreement over the entire energy range and additionally shows agreement in the resonance region. This indicates that this detector array may be used in the future to perform scattering resonance measurements. Last, at 150 deg there is good agreement above 4 keV; however, in the region from 4 to 2.5 keV, the experimental data are higher than any of the evaluations. This may indicate a region where all evaluations could improve. Overall, the experimental data agree well with the simulations in the region from 0.5 MeV to 2.5 keV.

VI. CONCLUSIONS

An experiment was performed to investigate the neutron scattering from a copper sample. The quasi-differential method was used to compare the experimental results to detailed MCNP simulations. Differences were found between the experiment and simulations in the high-energy region around 5 MeV for the ENDF evaluation at back angles and for all evaluations and at all angles in the region from 1 to 2 MeV. In the mid-energy region, there is a difference at 35 deg around 300 keV and at 150 deg in the region from 2.5 to 3.5 keV. These differences could indicate an issue in the evaluations in these regions, and a reevaluation utilizing these data is recommended. These changes could help to improve the agreement of the Zeus critical benchmarks.

Acknowledgments

This work was created while some of the authors were employed by the U.S. Government or one of its contractors,and with the scope of such employment, the U.S. Government is granted a non-exclusive royalty-free license topublish, republish, or reproduce the work or to allow others to reproduce this work for U.S. Government purposes.

The authors would like to thank the RPI LINAC staff: Peter Brand, Mathew Gray, Larry Krusieski, and Azeddine Kerdoun. The data presented in this publication would not have been possible without their time and effort. This work was partially supported by the Nuclear Criticality Safety Program, funded and managed by the National Nuclear Security Administration for the U.S. Department of Energy.

References

1. D. A. BROWN et al., "ENDF/B-VIII.0: The 8th Major Release of the Nuclear Reaction Data Library with Cielo-Project Cross Sections, New Standards and Thermal Scattering Data," *Nucl. Data Sheets*, **148**, 1 (2018).
2. A. J. M. PLOMPEN et al., "The Joint Evaluated Fission and Fusion Nuclear Data Library, JEFF-3.3," *Eur. Phys. J. A*, **56**, 181 (2020).
3. K. SHIBATA et al., "JENDL-4.0: A New Library for Nuclear Science and Engineering," *J. Nucl. Sci. Technol.*, **48**, *1*, 1 (2011); https://doi.org/10.1080/18811248.2011.9711675.
4. F. J. SAGLIME et al., "A System for Differential Neutron Scattering Experiments in the Energy Range from 0.5 to 20 MeV," *Nucl. Instrum. Meth. Phys. Res. A*, **620**, *2–3*, 401 (2010); https://doi.org/10.1016/j.nima.2010.04.051.
5. A. M. DASKALAKIS et al., "Quasi-Differential Elastic and Inelastic Neutron Scattering from Iron in the MeV Energy Range," *Ann. Nucl. Energy*, **110**, 603 (2017); https://doi.org/10.1016/j.anucene.2017.07.007.
6. A. DASKALAKIS et al., "Assessment of Beryllium and Molybdenum Nuclear Data Files with the RPI Neutron Scattering System in the Energy Region from 0.5 to 20 MeV," *EPJ Web Conf.*, **146**, 11037 (2017); https://doi.org/10.1051/epjconf/201714611037.
7. D. P. BARRY et al., "Quasi-Differential Neutron Scattering in Zirconium from 0.5 to 20 MeV," *Nucl. Sci. Eng.*, **172**, *2*, 188 (2013); https://doi.org/10.13182/NSE12-1.
8. A. E. YOUMANS et al., "Fast Neutron Scattering Measurements with Lead," *Trans. Am. Nucl. Soc.*, **115**, 355 (2015).
9. A. M. DASKALAKIS et al., "Quasi-Differential Neutron Scattering from ^{238}U from 0.5 to 20 MeV," *Ann. Nucl. Energy*, **73**, 455 (2014); https://doi.org/10.1016/j.anucene.2014.07.023.
10. R. CAPOTE et al., "Physics of Neutron Interactions with ^{238}U: New Developments and Challenges," *Nucl. Data Sheets*, **118**, 26 (2014); https://doi.org/10.1016/j.nds.2014.04.003.
11. V. SOBES and L. LEAL, "Results for the Intermediate-Spectrum Zeus Benchmark Obtained with New ^{63,65}Cu Cross-Section Evaluations," *Trans. Am. Nucl. Soc.*, **110**, 278 (2014).
12. J. D. BESS et al., "The 2019 Edition of the ICSBEP Handbook," Idaho National Laboratory (2019).
13. A. NOURI et al., "DICE: Database for the International Criticality Safety Benchmark Evaluation Program Handbook," *Nucl. Sci. Eng.*, **145**, *1*, 11 (2003); https://doi.org/10.13182/NSE03-15.
14. A. DASKALAKIS, "Measurement of Elastic and Inelastic Neutron Scattering in the Energy Range from 0.5 to 20 MeV," PhD Thesis, Rensselaer Polytechnic Institute (2015).
15. M. E. OVERBERG et al., "Photoneutron Target Development for the RPI Linear Accelerator," *Nucl. Instrum. Meth. Phys. Res. A*, **438**, *2*, 253 (1999); https://doi.org/10.1016/S0168-9002(99)00878-5.
16. J. T. GOORLEY et al. "Initial MCNP6 Release Overview – MCNP6 Version 1.0," LA-UR-13-22934, Los Alamos National Laboratory (2013).
17. M. B. CHADWICK et al., "ENDF/B-VII.1 Nuclear Data for Science and Technology: Cross Sections, Covariances, Fission Product Yields and Decay Data," *Nucl. Data Sheets*, **112**, *12*, 2887 (2011).